

# Supporting Information

## Cyclophospholipids enable a protocellular life cycle

*Ö. Duhan Toparlak,<sup>1,†</sup> Lorenzo Sebastianelli,<sup>2</sup> Veronica Egas Ortuno,<sup>3</sup> Megha Karki,<sup>3</sup>*

*Yanfeng Xing,<sup>4</sup> Jack W. Szostak,<sup>5,\*</sup> Ramanarayanan Krishnamurthy,<sup>3,\*</sup> and Sheref S.*

*Mansy,<sup>1,2,\*</sup>*

<sup>1</sup>Department of Cellular, Computational and Integrative Biology, University of Trento, Via Sommarive 9, 38123 Povo (TN), Italy

<sup>2</sup>Department of Chemistry, University of Alberta, 11227 Saskatchewan Drive, Edmonton AB T6G 2G2, Canada

<sup>3</sup>Department of Chemistry, The Scripps Research Institute, 10550 North Torrey Pines Road, La Jolla, CA 92037, USA

<sup>4</sup>Department of Biochemistry and Molecular Biology, University of Chicago, Chicago, IL 60637, USA

<sup>5</sup>Howard Hughes Medical Institute, Department of Chemistry, University of Chicago, Chicago, IL 60637, USA

<sup>†</sup>Current address: Department of Chemistry, University of Oxford, 12 Mansfield Road, Oxford, OX1 3TA, UK

## Table of Contents

- Figure S1.** Structures of chemicals used in this study.
- Figure S2.** Growth of CPC18-based protocells in the presence of  $\text{Mg}^{2+}$ -citrate.
- Figure S3.** Growth of CPC18-based protocells in the absence of  $\text{Mg}^{2+}$ -citrate.
- Figure S4.** Fatty acid (oleate) protocells did not grow in the presence of  $\text{Mg}^{2+}$ -citrate.
- Figure S5.** All MLVs failed to grow when fed with same composition of LUVs in the presence and absence of  $\text{Mg}^{2+}$ -citrate.
- Figure S6.** Growth and division of MLVs fed with LUVs.
- Figure S7.** Division of oleate-rich MLVs fed with CPC18-rich LUVs.
- Figure S8.** Comparing the division of oleate-rich admixture MLVs fed with pure CPC18 LUVs in the absence and presence of  $\text{Mg}^{2+}$ -citrate.
- Figure S9.** MLVs did not divide when fed with same composition of LUVs.
- Figure S10.** Calculations of hydrophobicity.
- Figure S11.** Entropic factors drive vesicle growth.
- Figure S12.** The direction of vesicle growth was controlled by differences in lipid concentration.
- Figure S13.** Probing the micellar fraction of CPC18-based vesicles.
- Figure S14.** Overview and raw data for desorption rate determination.
- Figure S15.** Sugar permeability profiles across various compositions of vesicle bilayers.
- Figure S16.** Purification of vesicles encapsulating oligonucleotides or small molecules.
- Figure S17.** Stability of cyclophospholipid-containing vesicles to pH and  $\text{Mg}^{2+}$ .
- Figure S18.** Growth and division of prebiotically plausible CPC10-based protocells in the absence of  $\text{Mg}^{2+}$ -citrate.
- Figure S19.** Growth and division of prebiotically plausible CPC10-based protocells in the presence of  $\text{Mg}^{2+}$ -citrate.
- Figure S20.** Release of small molecules and oligonucleotides from protocells.
- Figure S21.** NMR analysis of synthesized CPC10.
- Figure S22.** NMR analysis of synthesized CPC18.
- Table S1.** List of oligonucleotides and sequences used in this study.

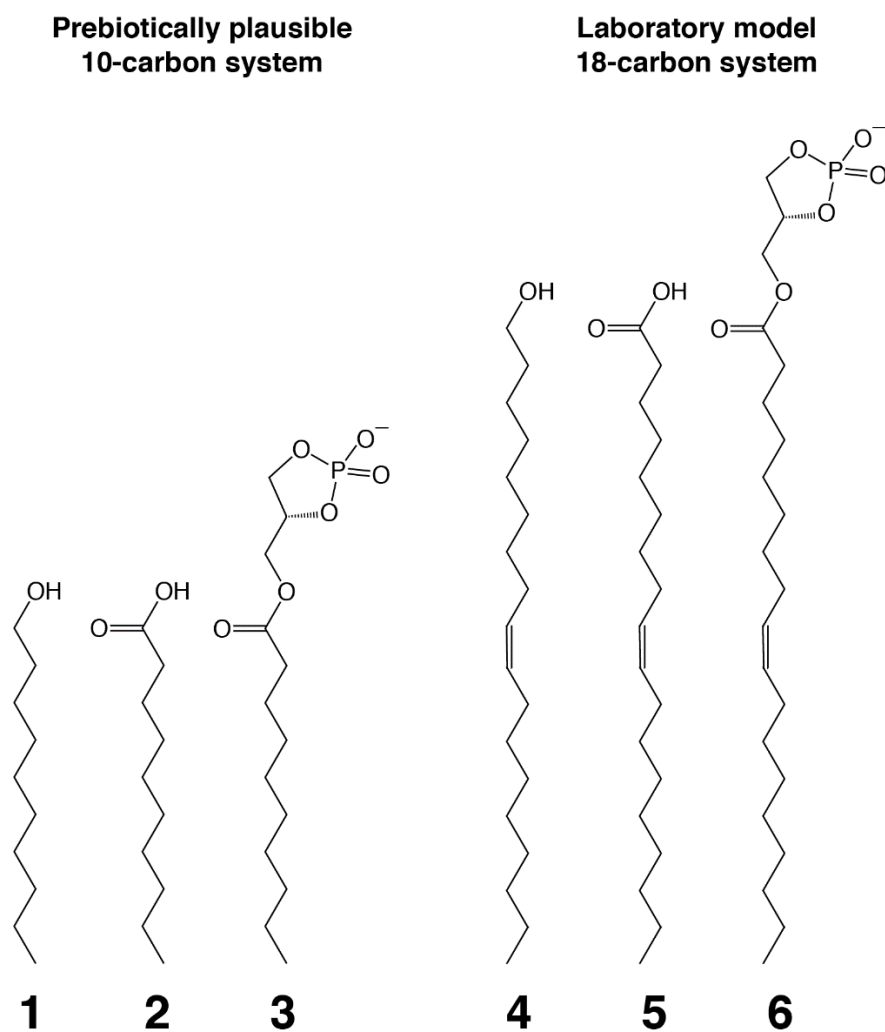


**Figure S1. Structures of chemicals used in this study.**

**1** decanol

**2** decanoic acid

**3** (2-hydroxy-2-oxido-1,3,2-dioxaphospholan-4-yl)methyl decanoate (cyclophospholipid C10, i.e. CPC10)

**4** oleyl alcohol

**5** oleic acid and

**6** (2-hydroxy-2-oxido-1,3,2-dioxaphospholan-4-yl)methyl oleate (cyclophospholipid C18:1, i.e. CPC18).

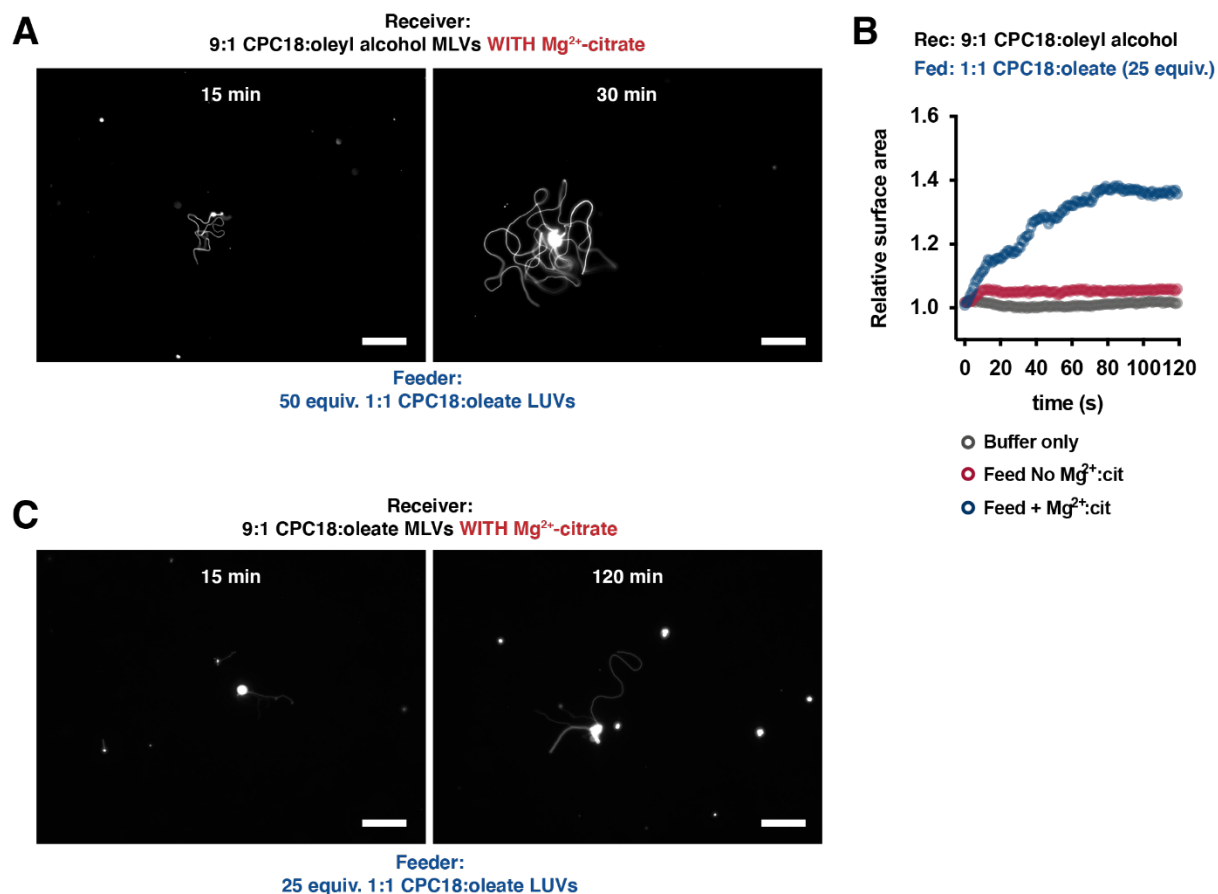


**Figure S2. Growth of CPC18-based protocells in the presence of  $Mg^{2+}$ -citrate.**

(A) 9:1 CPC18:oleyl alcohol MLVs fed with 50 equiv. 1:1 CPC18:oleate with  $Mg^{2+}$ -citrate.

(B) FRET-based assay monitoring of surface area changes in 9:1 CPC18:oleyl alcohol MLVs fed with 25 equiv. 1:1 CPC18:oleate with and without  $Mg^{2+}$ -citrate. Growth was more prominent in the presence of  $Mg^{2+}$ -citrate.

(C) 9:1 CPC18:oleate MLVs fed with 25 equiv. 1:1 CPC18:oleate with  $Mg^{2+}$ -citrate.

$Mg^{2+}$ -citrate indicates 25 mM  $Mg^{2+}$ , 100 mM citrate. All images were taken from different fields and scale bars indicate 20  $\mu$ m. For fluorescence imaging, the vesicles were labeled with 0.15 mol% LR-DHPE.

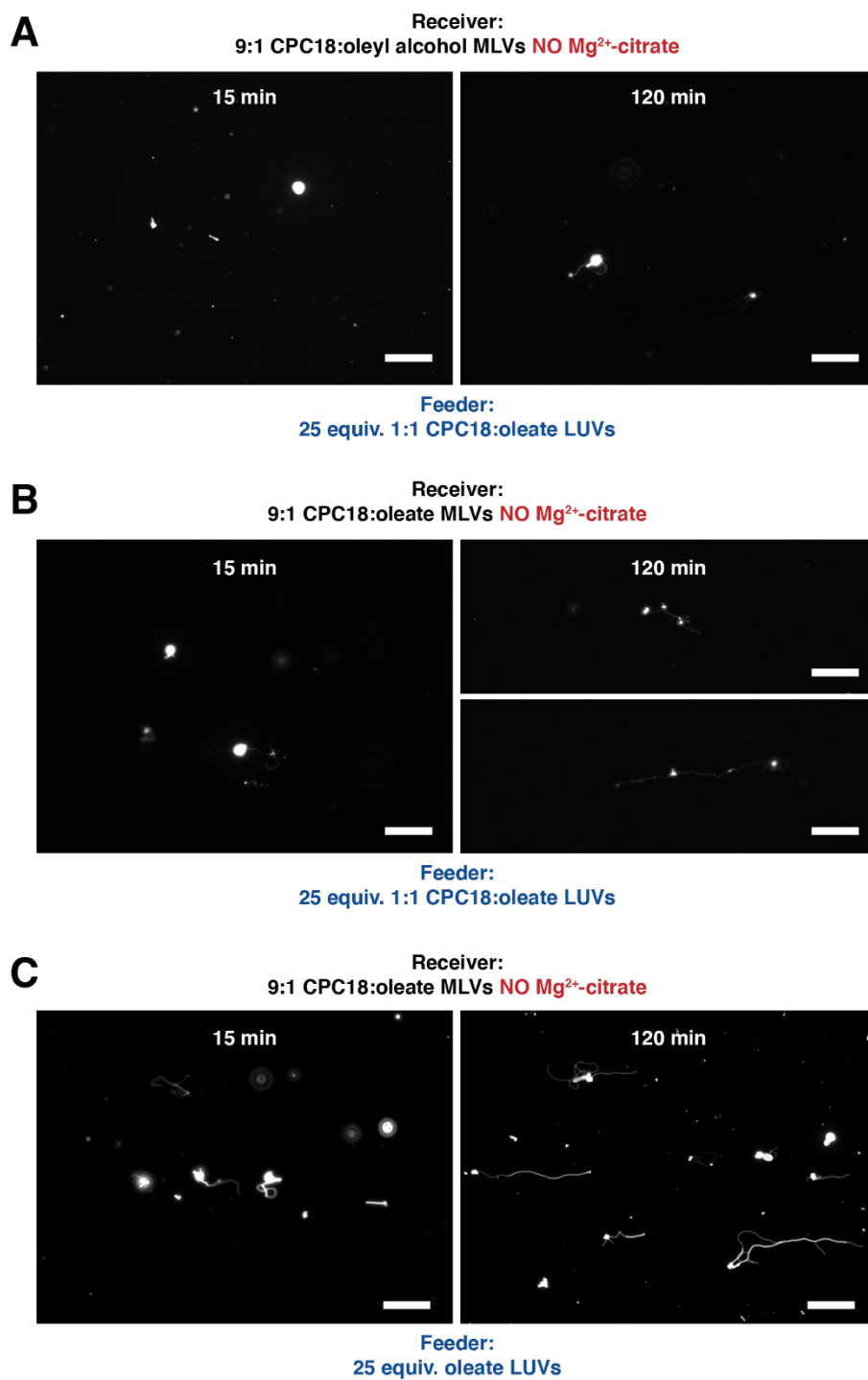


**Figure S3. Growth of CPC18-based protocells in the absence of Mg<sup>2+</sup>-citrate.**

**(A)** 9:1 CPC18:oleyl alcohol MLVs fed with 25 equiv. 1:1 CPC18:oleate LUVs.

**(B)** 9:1 CPC18:oleate MLVs fed with 25 equiv. 1:1 CPC18:oleate LUVs.

**(C)** 9:1 CPC18:oleate MLVs fed with 25 equiv. oleate LUVs.

All images were taken from different fields and scale bars indicate 20  $\mu\text{m}$ . For fluorescence imaging, the vesicles were labeled with 0.15 mol% LR-DHPE.

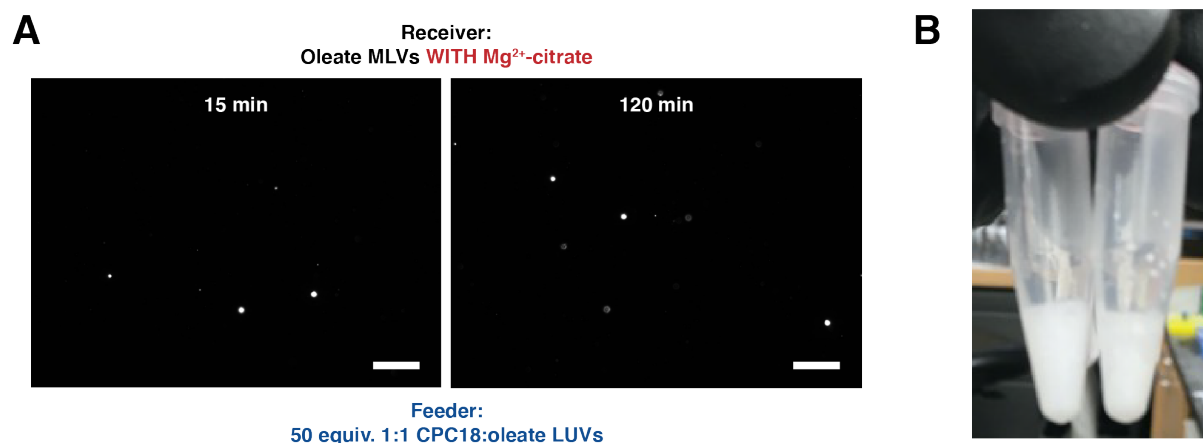


**Figure S4. Fatty acid (oleate) protocells did not grow in the presence of Mg<sup>2+</sup>-citrate.**

**(A)** 1:0 oleate MLVs fed with 50 equiv. 1:1 CPC18:oleate LUVs. For fluorescence imaging, the vesicles were labeled with 0.15 mol% LR-DHPE.

**(B)** Image of the preparation of oleate micelles (50 mM) in the presence of 25 mM Mg<sup>2+</sup>-citrate Mg<sup>2+</sup>-citrate, at pH > 10. Micelle solutions are clear (15). The white solid precipitate was consistent with the presence of magnesium hydroxide and aggregates of fatty acid. 1:4 Mg<sup>2+</sup>-citrate was prepared according to past reports (37) and was prepared at least 1 h before addition to solution. Images were taken from different fields and scale bars indicate 20  $\mu$ m.

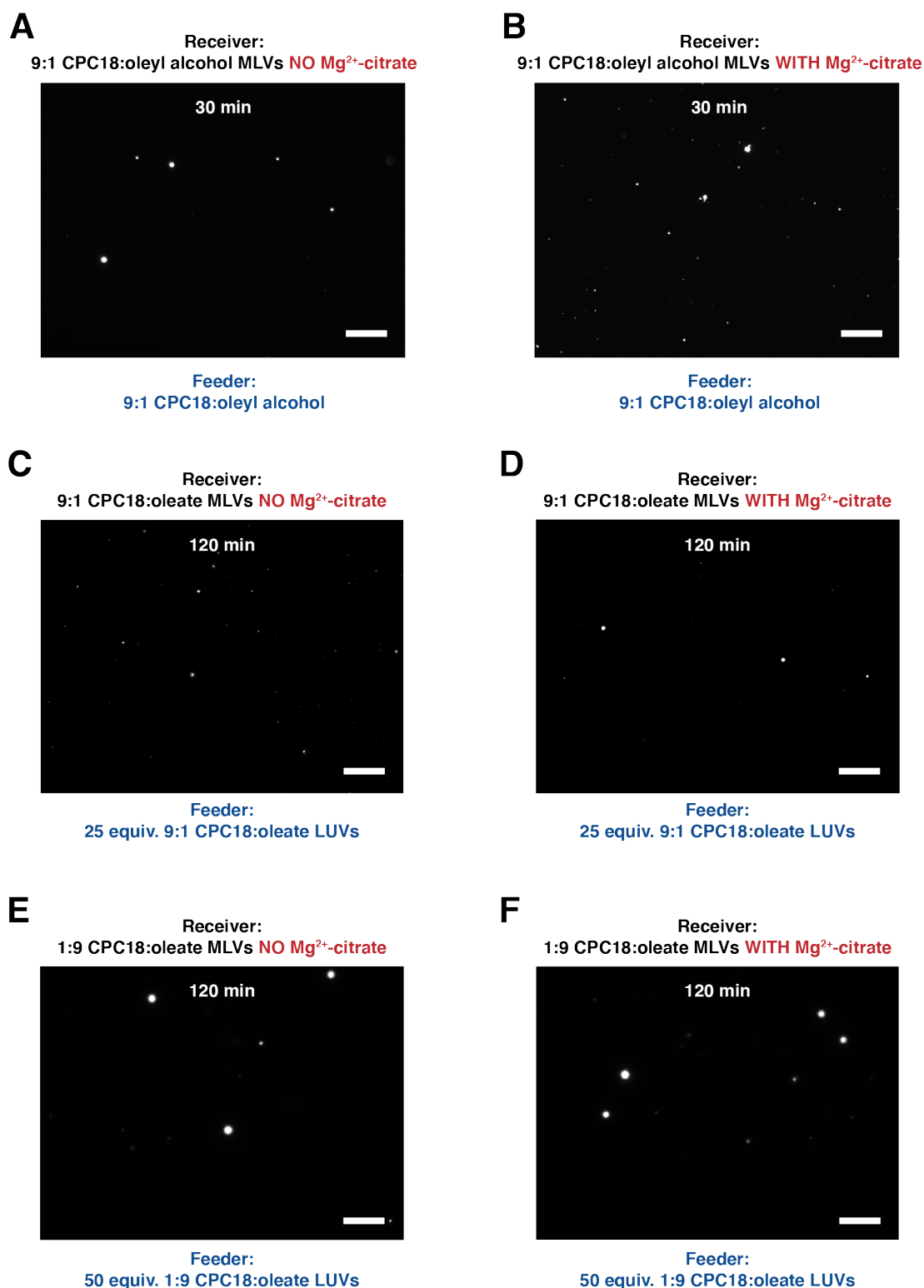


**Figure S5. All MLVs failed to grow when fed with same composition of LUVs both in the presence and absence of  $\text{Mg}^{2+}$ -citrate.**

(A, B) 9:1 CPC18:oleyl alcohol MLVs were fed with the same composition of LUVs.

(C, D) 9:1 CPC18:oleate MLVs were fed with the same composition of LUVs.

(E, F) 1:9 CPC18:oleate MLVs were fed with the same composition of LUVs.

$\text{Mg}^{2+}$ -citrate indicates 25 mM  $\text{Mg}^{2+}$ , 100 mM citrate. All images were taken from different fields. Scale bars indicate 20  $\mu\text{m}$ . For fluorescence imaging, the vesicles were labeled with 0.15 mol% LR-DHPE.

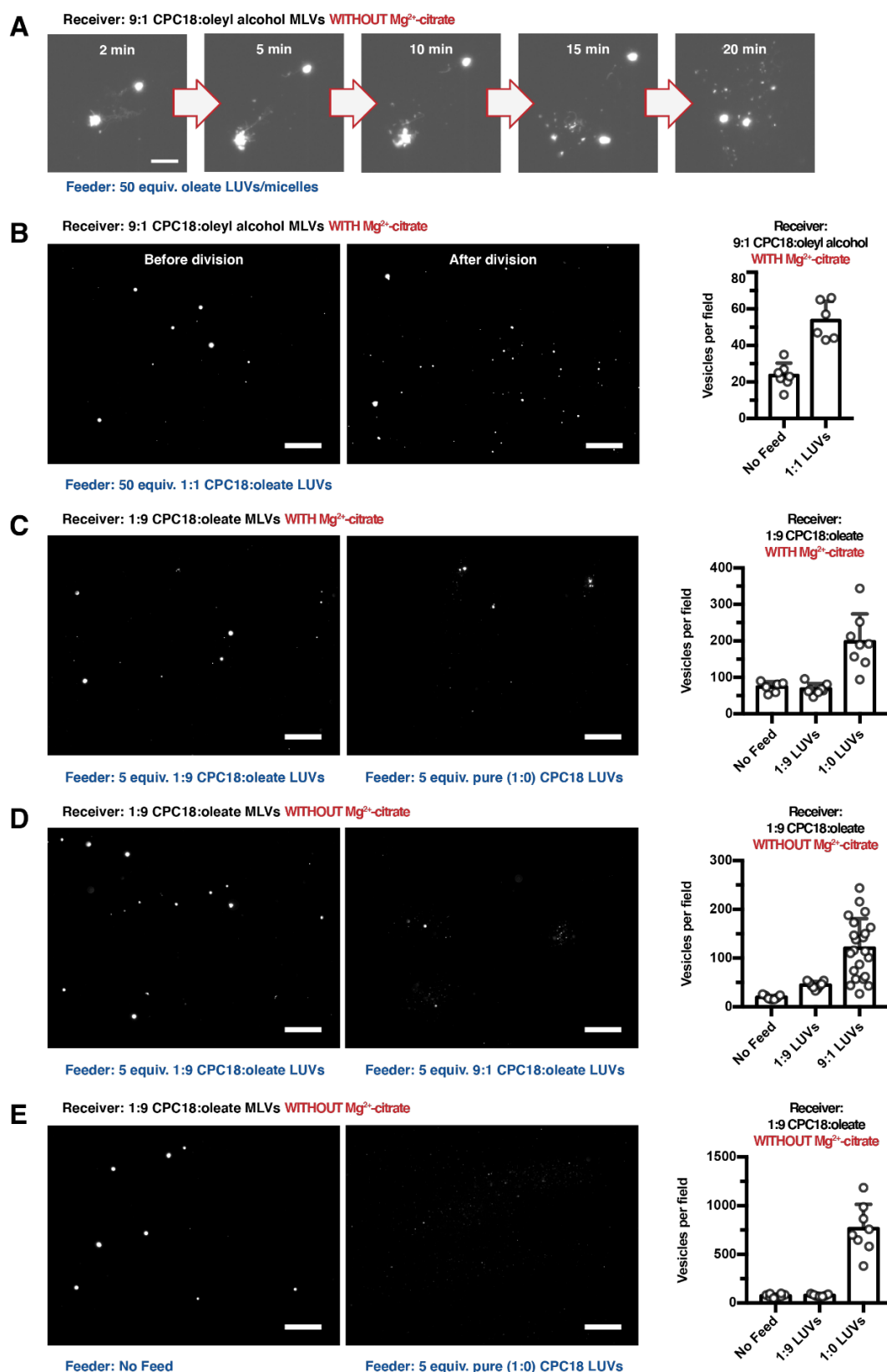


**Figure S6. Growth and division of MLVs fed with LUVs.**

**(A)** Growth and division of 9:1 CPC18:oleyl alcohol MLVs fed with pure oleate LUVs.

**(B–E)** Growth, division, and vesicle counting analyses of various MLV compositions.

The images are from different fields except (A). Scale bars indicate 20  $\mu$ m.  $Mg^{2+}$ -citrate indicates 25 mM  $Mg^{2+}$ , 100 mM citrate. For fluorescence imaging, the vesicles were labeled with 0.15 mol% LR-DHPE.



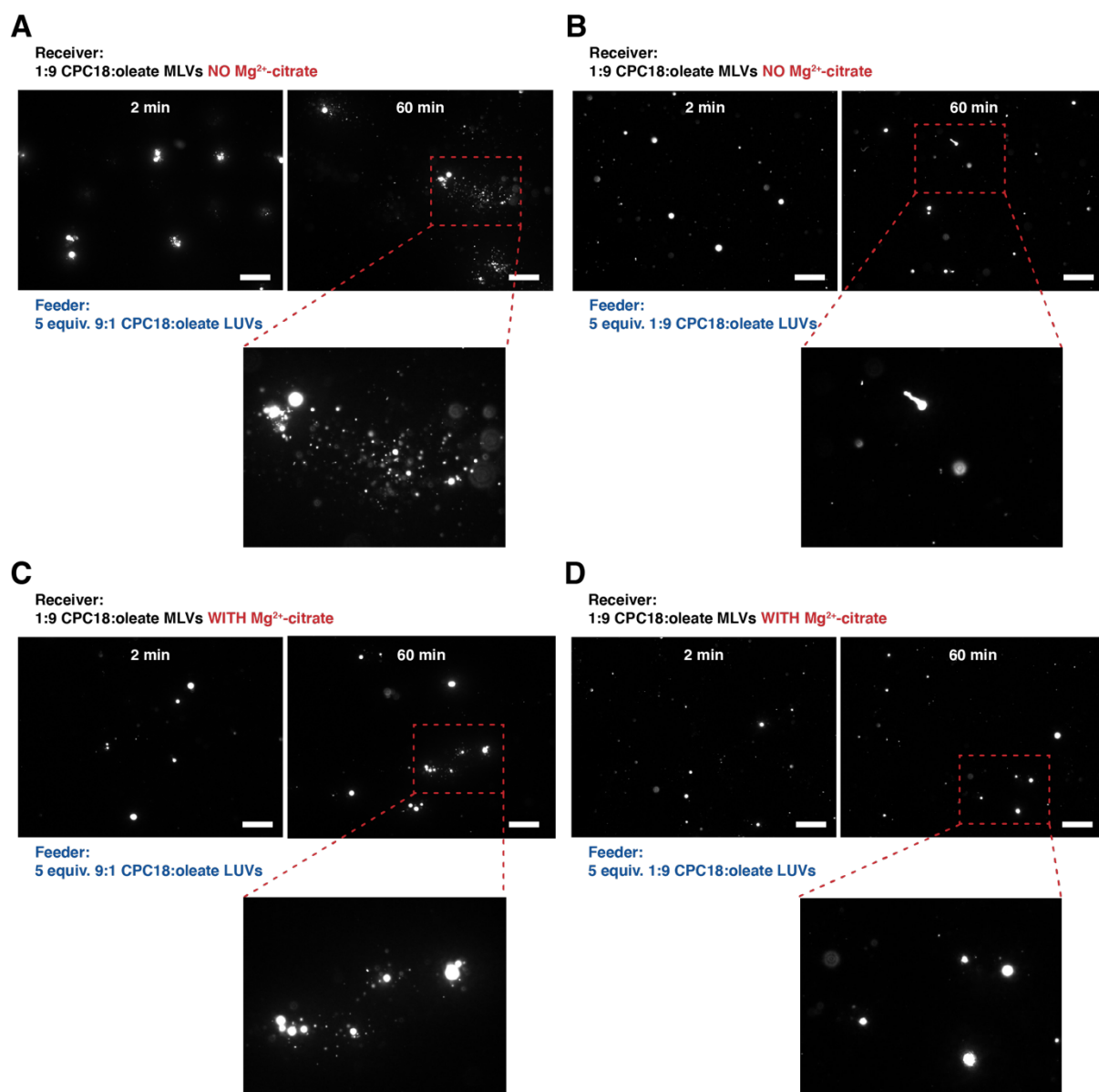


**Figure S7. Division of oleate-rich MLVs fed with CPC18-rich LUVs.**

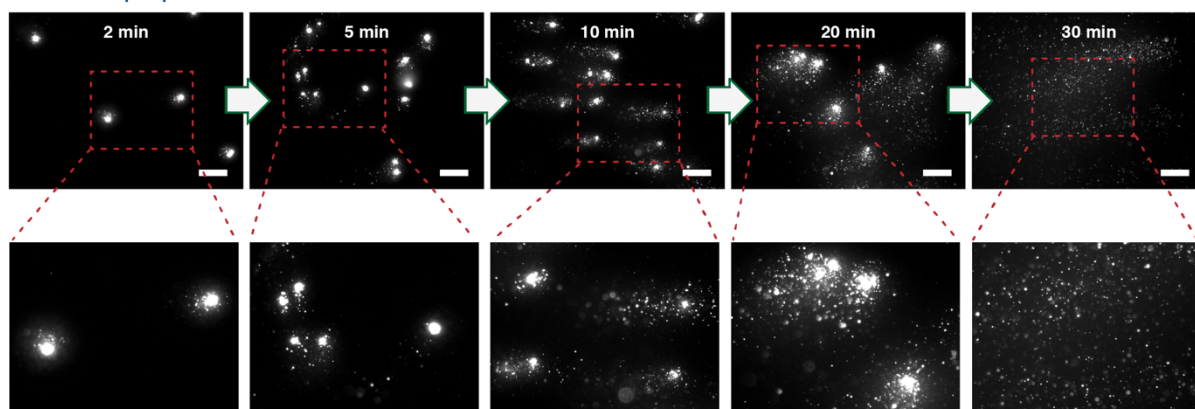
**(A)** 1:9 CPC18:oleate MLVs divided when fed with CPC18-rich LUVs in the absence of  $\text{Mg}^{2+}$ -citrate.  
**(B)** 1:9 CPC18:oleate MLVs did not divide when fed with CPC18-rich LUVs in the absence of  $\text{Mg}^{2+}$ -citrate.

**(C)** 1:9 CPC18:oleate MLVs divided when fed with CPC18-rich LUVs in the presence of  $\text{Mg}^{2+}$ -citrate.  
**(D)** 1:9 CPC18:oleate MLVs did not divide when fed with CPC18-rich LUVs in the presence of  $\text{Mg}^{2+}$ -citrate.

$\text{Mg}^{2+}$ -citrate indicates 25 mM  $\text{Mg}^{2+}$ , 100 mM citrate. Images were taken from different fields. Scale bars indicate 20  $\mu\text{m}$ . For fluorescence imaging, the vesicles were labeled with 0.15 mol% LR-DHPE.

**A**Receiver: 1:9 CPC18:oleate MLVs **NO**  $\text{Mg}^{2+}$ -citrate

Feeder: 5 equiv. pure CPC18 LUVs

**B**Receiver: 1:9 CPC18:oleate MLVs **WITH**  $\text{Mg}^{2+}$ -citrate

Feeder: 5 equiv. pure CPC18 LUVs

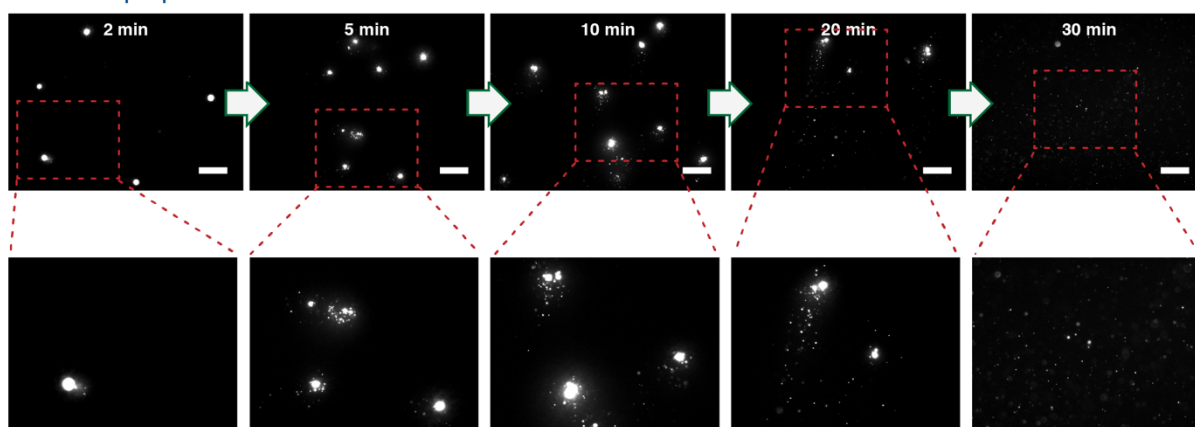


**Figure S8. Comparing the division of oleate-rich MLVs fed with pure CPC18 LUVs in the absence and presence of  $\text{Mg}^{2+}$ -citrate.**

**(A)** 1:9 CPC18:oleate MLVs divided when fed with pure CPC18 LUVs in the absence of  $\text{Mg}^{2+}$ -citrate.

**(B)** 1:9 CPC18:oleate MLVs divided when fed with pure CPC18 LUVs in the presence of  $\text{Mg}^{2+}$ -citrate.

$\text{Mg}^{2+}$ -citrate indicates 25 mM  $\text{Mg}^{2+}$ , 100 mM citrate. Images were taken from different fields. Scale bars indicate 20  $\mu\text{m}$ . For fluorescence imaging, the vesicles were labeled with 0.15 mol% LR-DHPE.

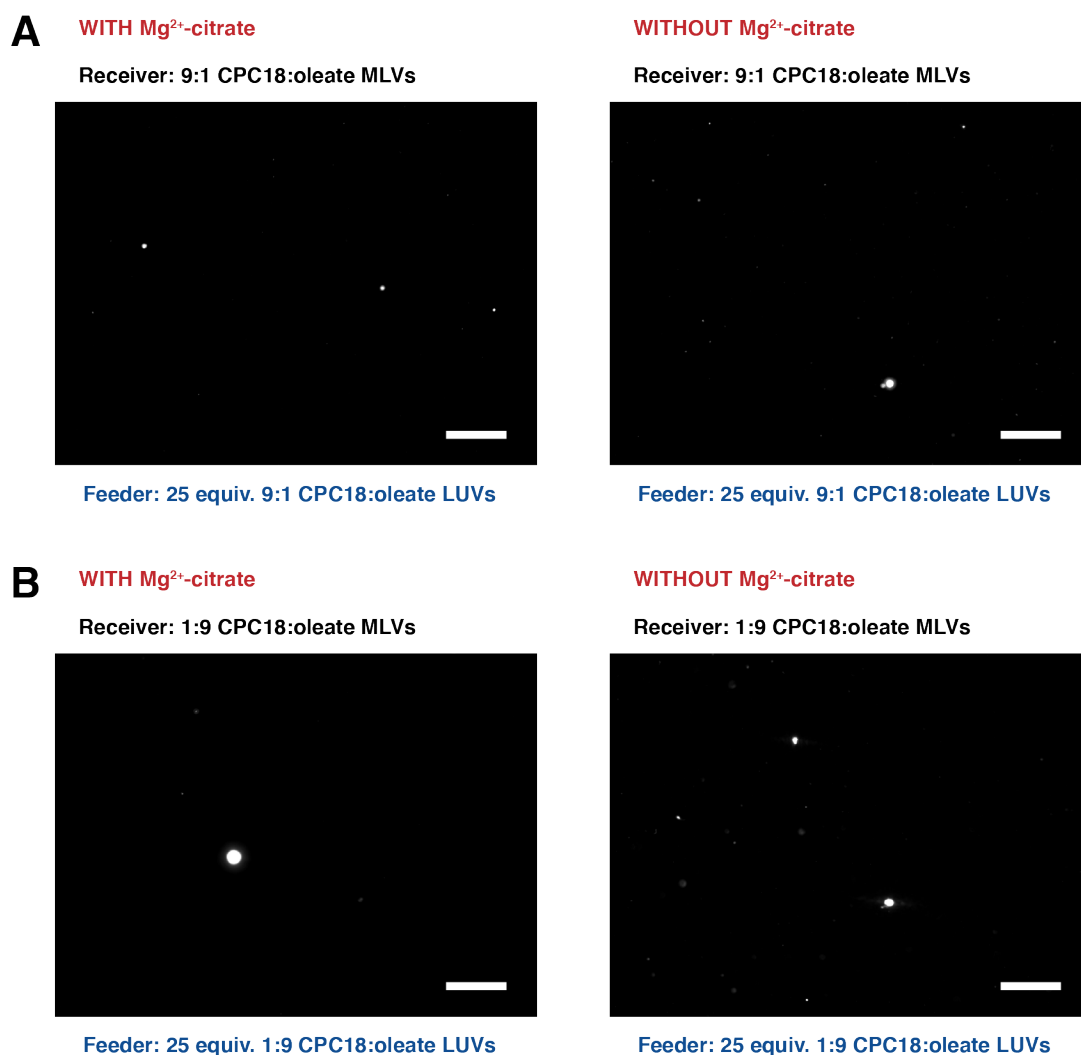


**Figure S9. MLVs did not divide when fed with same composition of LUVs.**

(A) Monitoring of 9:1 CPC18:oleate MLVs at 30 min when fed with LUVs of the same composition.  
(B) Monitoring of 1:9 CPC18:oleate MLVs at 30 min when fed with LUVs of the same composition.  
 $Mg^{2+}$ -citrate indicates 25 mM  $Mg^{2+}$ , 100 mM citrate. All images were taken from different fields and scale bars indicate 20  $\mu$ m. For fluorescence imaging, the vesicles were labeled with 0.15 mol% LR-DHPE.

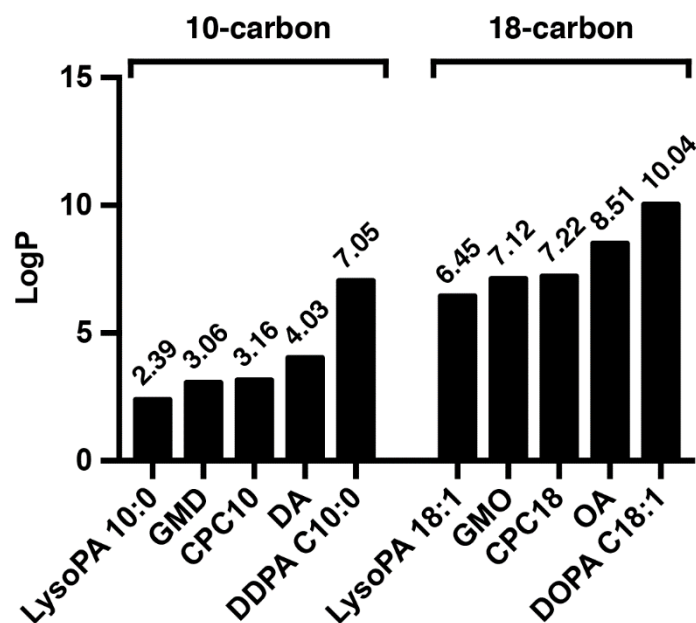


**Figure S10. Calculations of hydrophobicity.**

Membrane hydrophobicities based on theoretical calculations of octanol-water partition coefficients (logP). LysoPA, lysophosphatidic acid (single-chain); GMD, glycerylmonodecanoate (monocaprin); DA, decanoic acid; DDPA, didecanoylphosphatidic acid (double-chain); GMO, glyceryl monooleate (monoolein); OA, oleate; DOPA, dioleoylphosphatidic acid. Calculations were with Molinspiration Property Calculation Service ([www.molinspiration.com](http://www.molinspiration.com)). Greater values indicate increased hydrophobicity.

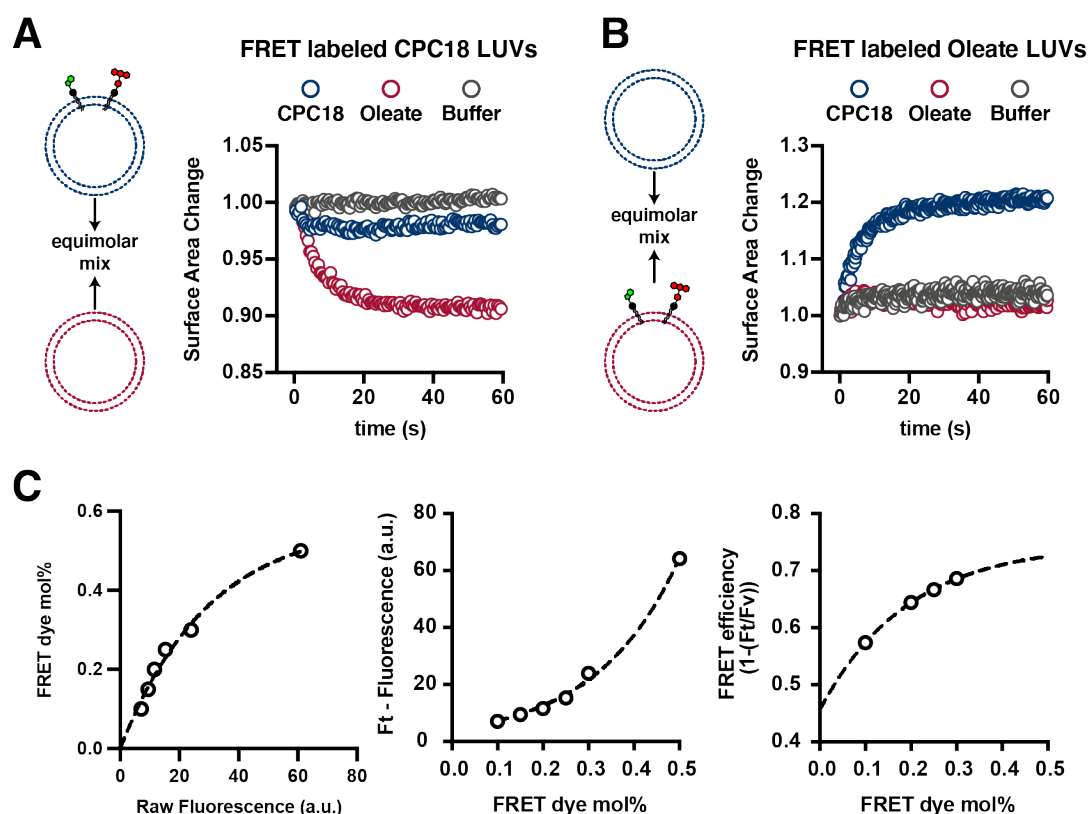


**Figure S11. Entropic factors drive vesicle growth.**

**(A-B)** Determination of bilayer preference of cyclophospholipids (CPC18) and fatty acids (oleate) in equimolar mixtures. FRET-based surface area and FRET fluorescence signal changes were determined in mixtures of cyclophospholipids and fatty acids competing with each other. Surface area decrease in CPC18 LUVs (A) and surface area increase in oleate LUVs (B) revealed that CPC18 preferred to enter into oleate bilayers within first 1-2 min of monitoring. The details of the kinetic assay are provided in Fig. 1A. Arbitrary spikes in the early phases of fluorimeter readings were excluded in the final data presentation for clarity, which arose due to pipetting and mixing in the cuvette.

**(C)** Calibration curves for the FRET-based surface area assay. *Left:* Raw FRET fluorescence measurements with vesicles with various mol% dyes. The curve fitting was applied to one-phase association with  $Y_0=0$ , and following values were found: plateau=0.57,  $K=0.033$ , with  $R^2=0.98$  for the formula of  $Y=Y_0 + (\text{Plateau}-Y_0) \cdot (1-e^{-K \cdot x})$ . *Center:* FRET dye mol% validation with respect to fluorescence of triton (Ft) added vesicles 1 mol% (v/v). Exponential equation curve fitting was applied,  $R^2=0.99$  was found. *Right:* FRET dye mol% with respect to FRET efficiency, standard curve. One-phase association curve fitting was applied,  $R^2=0.99$  was found.

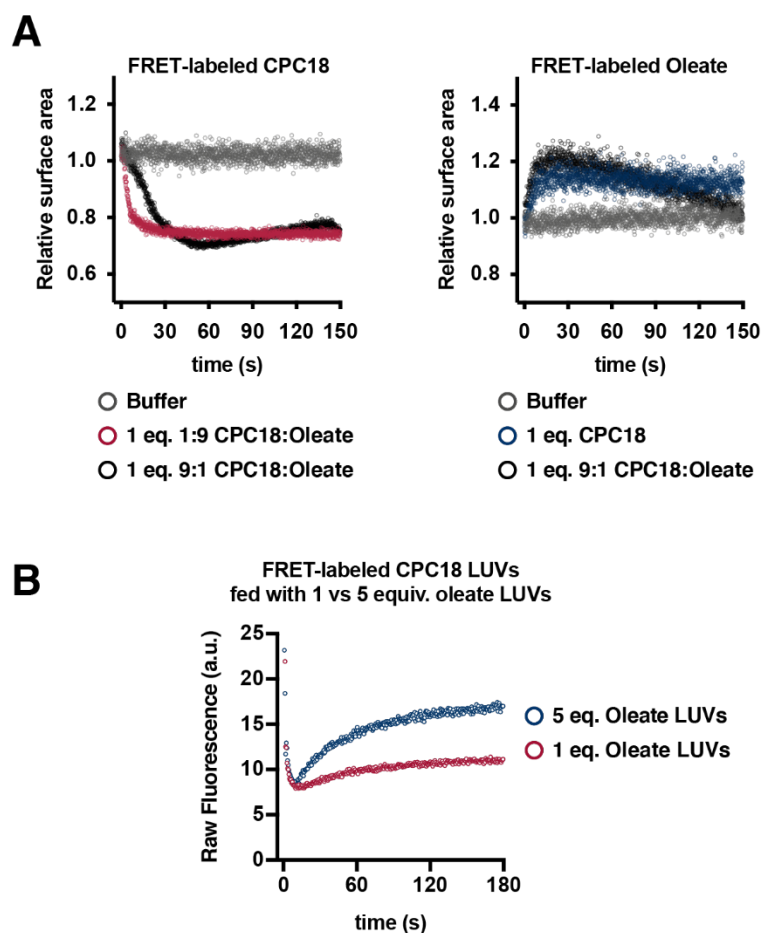


**Figure S12. The direction of vesicle growth was controlled by differences in lipid concentration.**

**(A)** The growth of FRET-labeled oleate or FRET-labeled CPC18 LUVs fed with various compositions of LUVs.

**(B)** Raw data for the growth of CPC18 LUVs with excess oleate LUVs. Note that the decrease in fluorescence indicates dilution of the FRET dye pair, thus indicating membrane growth. The increase in fluorescence, on the contrary, suggests the shrinkage of the vesicles. Here, the FRET-labeled vesicles first grew rapidly and then subsequently lost lipids. The initial growth phase may have been due to adsorption of CPC18 micelles to the surface of the oleate LUVs. The background fluorescence levels due to increased turbidity were normalized to 1 equiv. value by subtracting the corresponding difference from the 5 equiv. data.

In all tests, arbitrary spikes in the early phases of fluorimeter readings were excluded in the final data presentation, which arose due to pipetting and mixing in the cuvette.

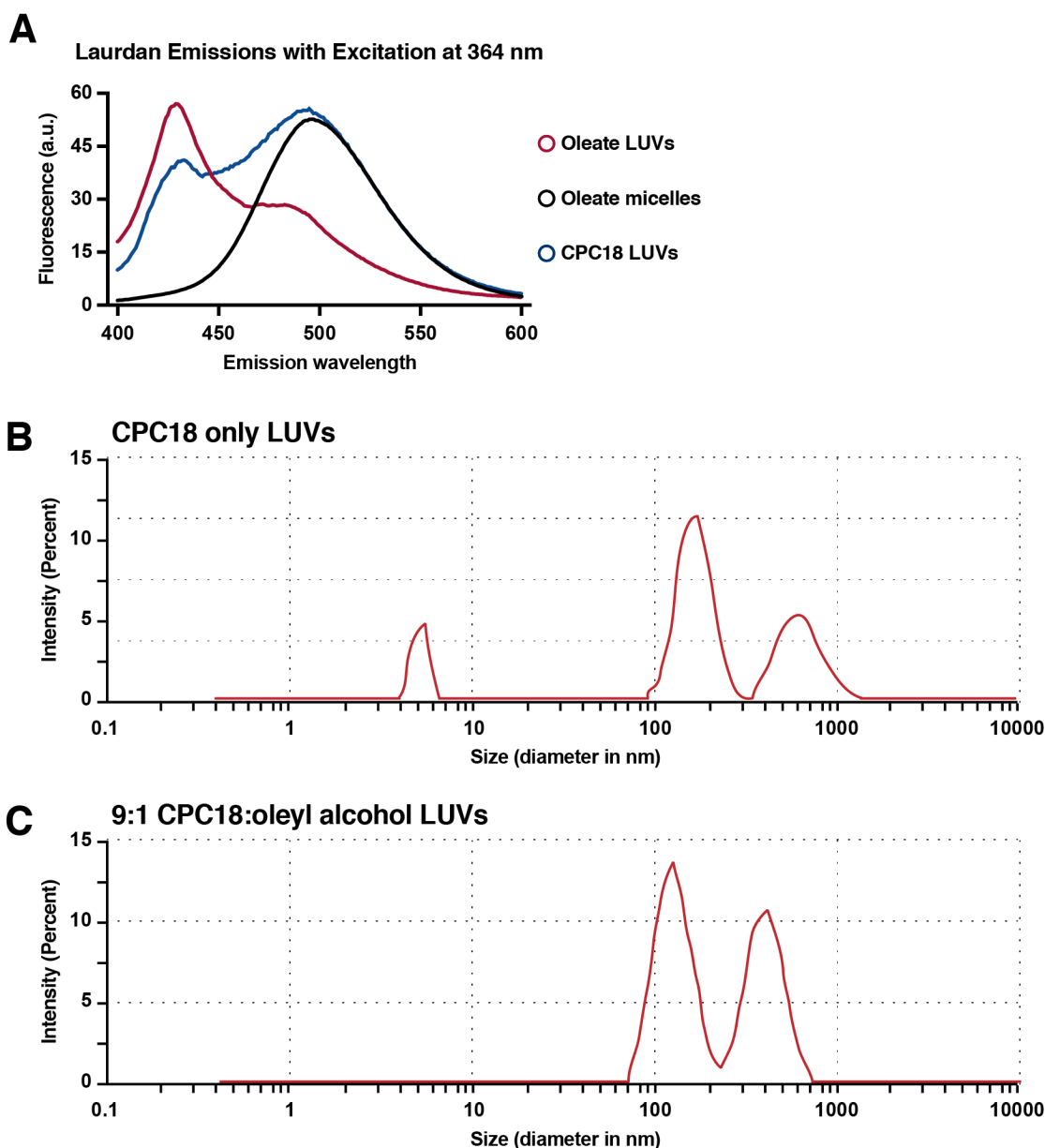


**Figure S13. Probing the micellar fraction of CPC18-based vesicles.**

**(A)** Determination of the dynamic equilibrium conditions in solution with the hydrophobic fluorescent probe Laurdan. Laurdan provides greater monomer polarization and a characteristic 500 nm emission peak if a micellar fraction exists. Note that in CPC18 LUVs, both vesicle (435 nm) and micelle (500 nm) emission peaks exist.

**(B)** Dynamic Light Scattering (DLS) measurements of pure CPC18 LUVs at 2 mM (above CVC), indicated characteristic 3-4 nm micellar peak, while the rest of the molecules were in dynamic equilibrium with large and small vesicles of diameters ranging from hundreds to a few thousands of nanometers.

**(C)** The DLS measurements of mixed 9:1:oleyl alcohol CPC18 LUVs, at 2 mM (above CVC) resulted in diminishing characteristic 3-4 nm micellar peak, while the rest of the molecules were still in dynamic equilibrium with large and small vesicles of diameters ranging from hundreds to a few thousands of nanometers.

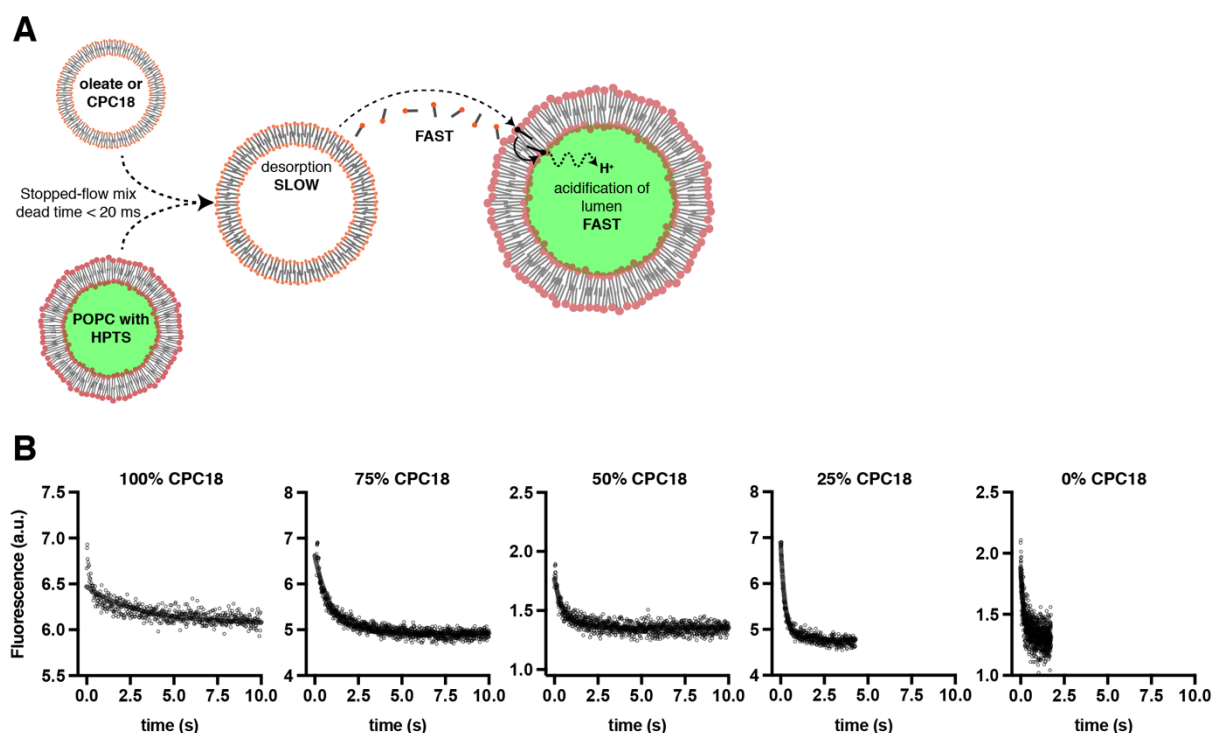


**Figure S14. Overview and raw data for desorption rate determination.**

**(A)** Breakdown of molecular events for the desorption rate determination assay by using the pH-sensitive probe 8-hydroxypyrene-1,3,6-trisulfonic acid (HPTS). HPTS shows a major excitation peak from 405 nm at pH 7.0 to 454 nm at pH 8.0. That is, since all flip-flop events at the bilayer will take place in the protonated form of the lipids, the flip-flop motion will result with ultimate acidification of the reporter POPC vesicle interior. This way, the drop in pH values is recorded and the individual curves are fit for one-phase decay kinetics. The value of the rate constant provides the rate of desorption. This is because the timeframes of stopped-flow mixing and monomer flip-flop, as well as the time spent by the individual monomer in bulk solution is theoretically assumed on the order of milliseconds to microseconds. Therefore, the eventual net observation is the pH-gradient decay by the flip-flop of the lipids. However, if the flip-flop motion is also slow and is on par with actual desorption rates (ca. order-of-magnitude higher than the initial estimates), the desorption rates might be underestimated.

**(B)** Representative, individual measurements of the pH-gradient decay in various compositions of vesicles. The data were fit to one-phase decay with  $R^2 \geq 0.55$



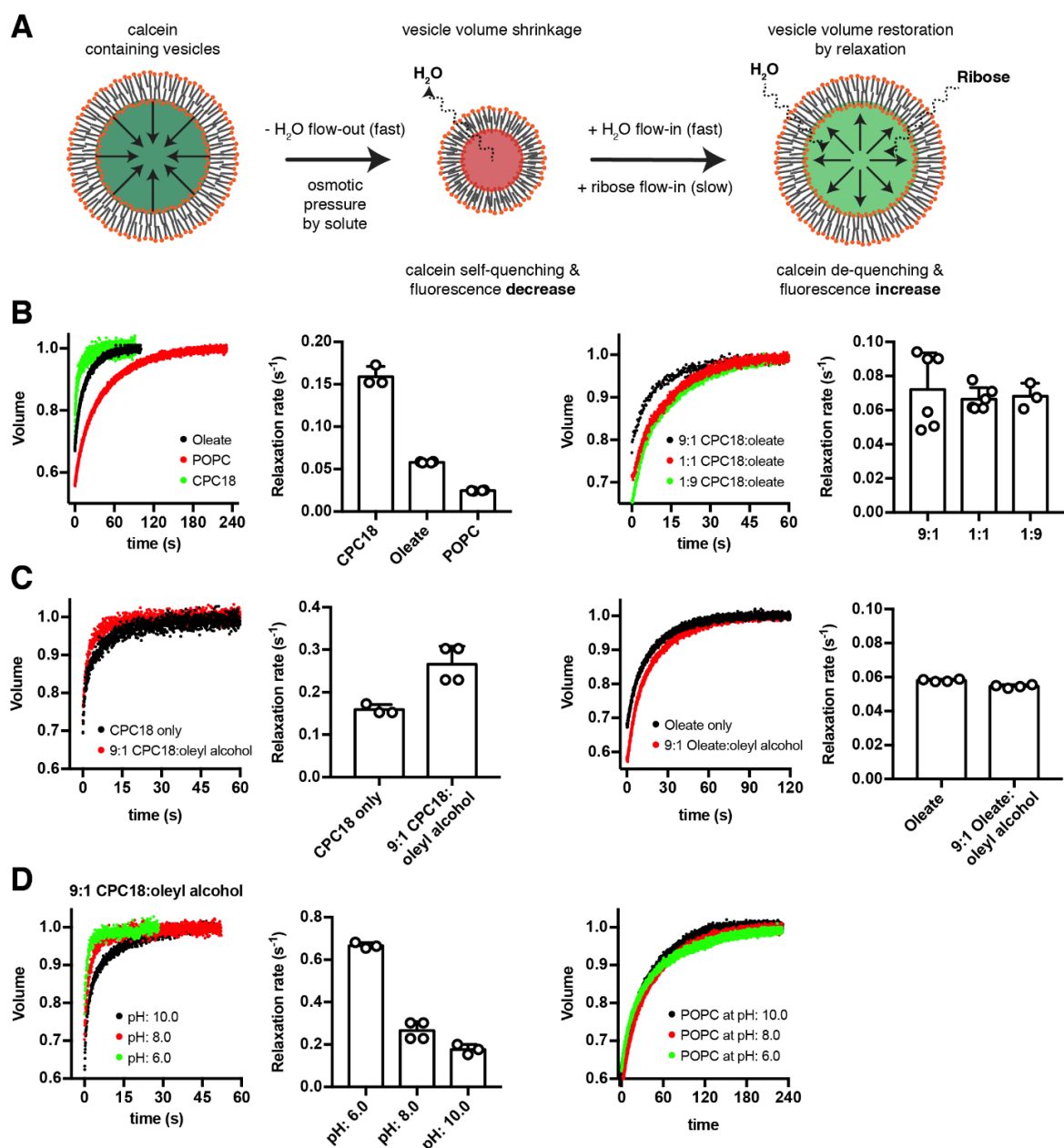


**Figure S15. Ribose permeability profiles across various compositions of vesicle bilayers.**

**(A)** Cartoon representation of shrink-swell assay for sugar permeability in self-quenching calcein encapsulating vesicles. The calcein was provided as 10 mM and solutes were provided in 0.5 M final concentrations. Within few milliseconds, water effluxes the vesicles due to osmotic pressure by the surrounding sugar solution, the vesicles shrink in size and the encapsulated calcein concentrations increase to self-quenching levels. Subsequently, the solute permeation restores the original volume of the vesicles, as the water rushes in along with the solute. The osmotic shock is slowly alleviated by the equilibration of the solutes in and out of the bilayers, while the calcein fluorescence is gradually rescued from the self-quenching, resulting in characteristic logarithmic curve of the volume increase.

**(B)** D-Ribose permeability comparison between different vesicle compositions at pH 8. POPC stands for phospholipid 1-palmitoyl-2-oleoyl-sn-glycero-3-phosphocholine.

**(C)** The presence of nontitratable hydrogen-bond donor changes the membrane permeability profile of CPC18-based vesicles but not of oleate-based vesicles at pH 8.

**(D)** The buffer pH influences the membrane permeability profile of cyclophospholipid-based vesicles, but not of POPC vesicles. The apparent pK<sub>a</sub> of CPC18 is above 4 (ref. 72 in main text). All data were collected with  $n \geq 3$  replicates and the plots show  $\pm$ SD.

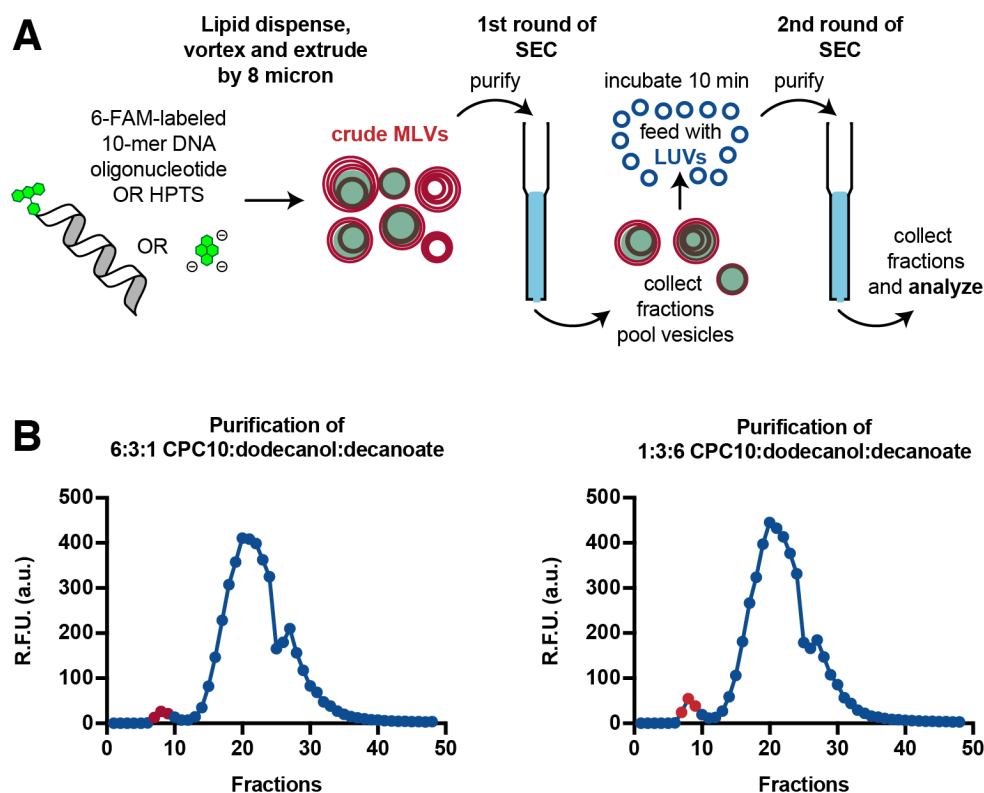


**Figure S16. Purification of vesicles encapsulating oligonucleotides or small molecules.**

**(A)** Cartoon representation of the events. Size-exclusion chromatography (SEC) was run on the crude multilamellar vesicles (MLVs) that were extruded to 8  $\mu\text{m}$  to remove the lipid aggregates. The MLVs were purified on Sepharose 4B resin and fractions were collected in a 96-well plate with an automated fraction collector.

**(B)** Example purification data. Only the first 3-4 vesicle-containing fractions (red labeled) were collected and tested for growth and division studies. Here, fluorescence was from FAM-labeled 10-mer DNA oligonucleotide (dC10) with excitation and emission wavelengths of 485 nm and 515 nm, respectively.

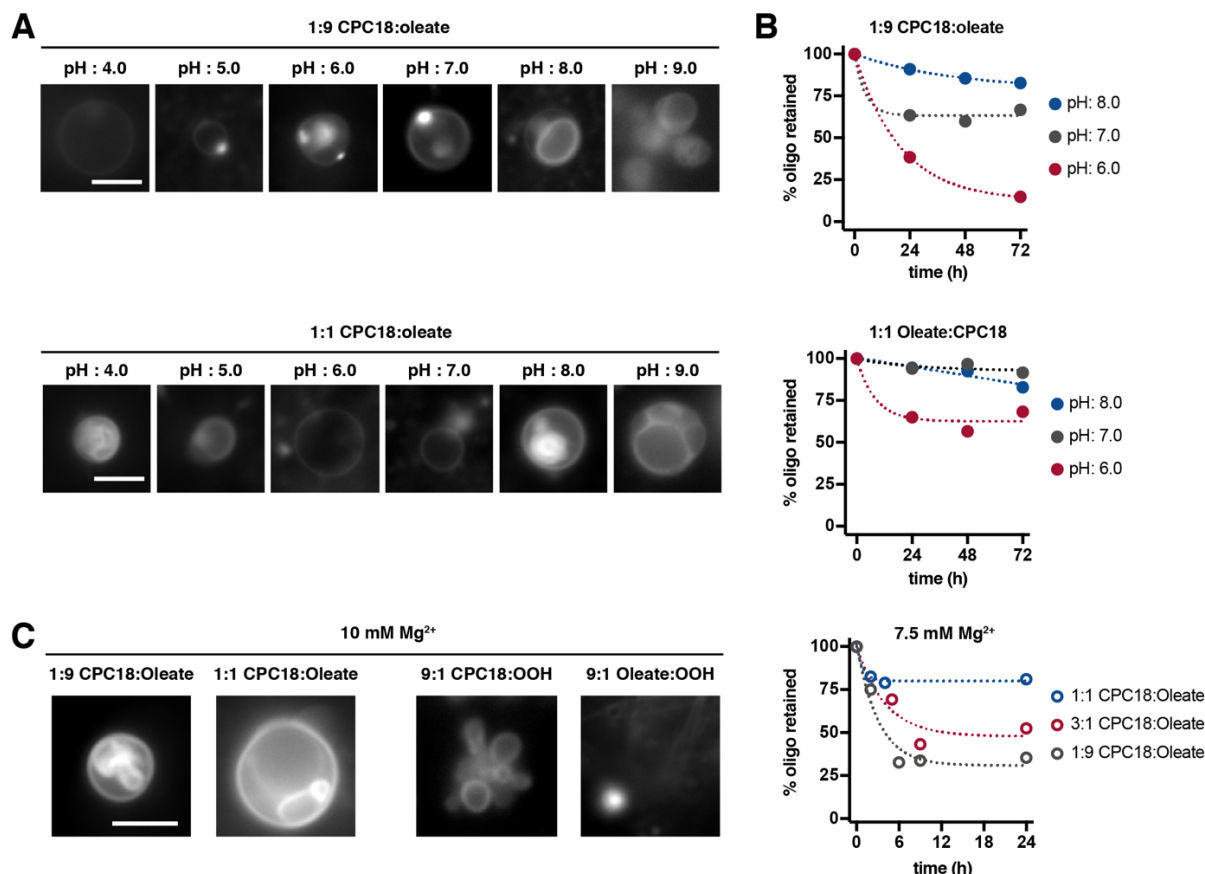


**Figure S17. Stability of cyclophospholipid-containing vesicles to pH and Mg<sup>2+</sup>.**

**(A)** The vesicles were subjected to a range of pH for microscopic analysis as well as retainment of encapsulated fluorescein-labeled 10-mer DNA oligonucleotide. The tested vesicles were LUVs.

**(B)** Vesicle stability over 72 h at different CPC18:oleate molar ratios and pH. Fluorescence was from FAM-labeled 10-mer DNA oligonucleotide (dA10) with excitation and emission wavelengths of 485 nm and 515 nm, respectively.

**(C)** Vesicle stability to unchelated 10 mM and 7.5 mM Mg<sup>2+</sup>. OOH stands for oleyl alcohol.

The vesicles were increasingly less pronounced with decreasing pH. For pH 4.0 and 5.0, citrate buffer; for pH 6.0, MES buffer; for pH 7.0 and 8.0 HEPES buffer and for pH 9.0, carbonate/bicarbonate buffers were used at 0.2 M concentrations. In all cases, the pH was adjusted either by ratios of the donor and acceptors (citrate and carbonate systems) or by 5 M NaOH (MES and HEPES systems). The Mg<sup>2+</sup> experiments were performed with 0.2 M Na<sup>+</sup>-HEPES, pH 7.5. The vesicles were imaged without purification at t = 10 min. All images were taken from different fields and scale bars indicate 10  $\mu$ m. For fluorescence imaging, the vesicles were labeled with 10  $\mu$ M rhodamine 6G.

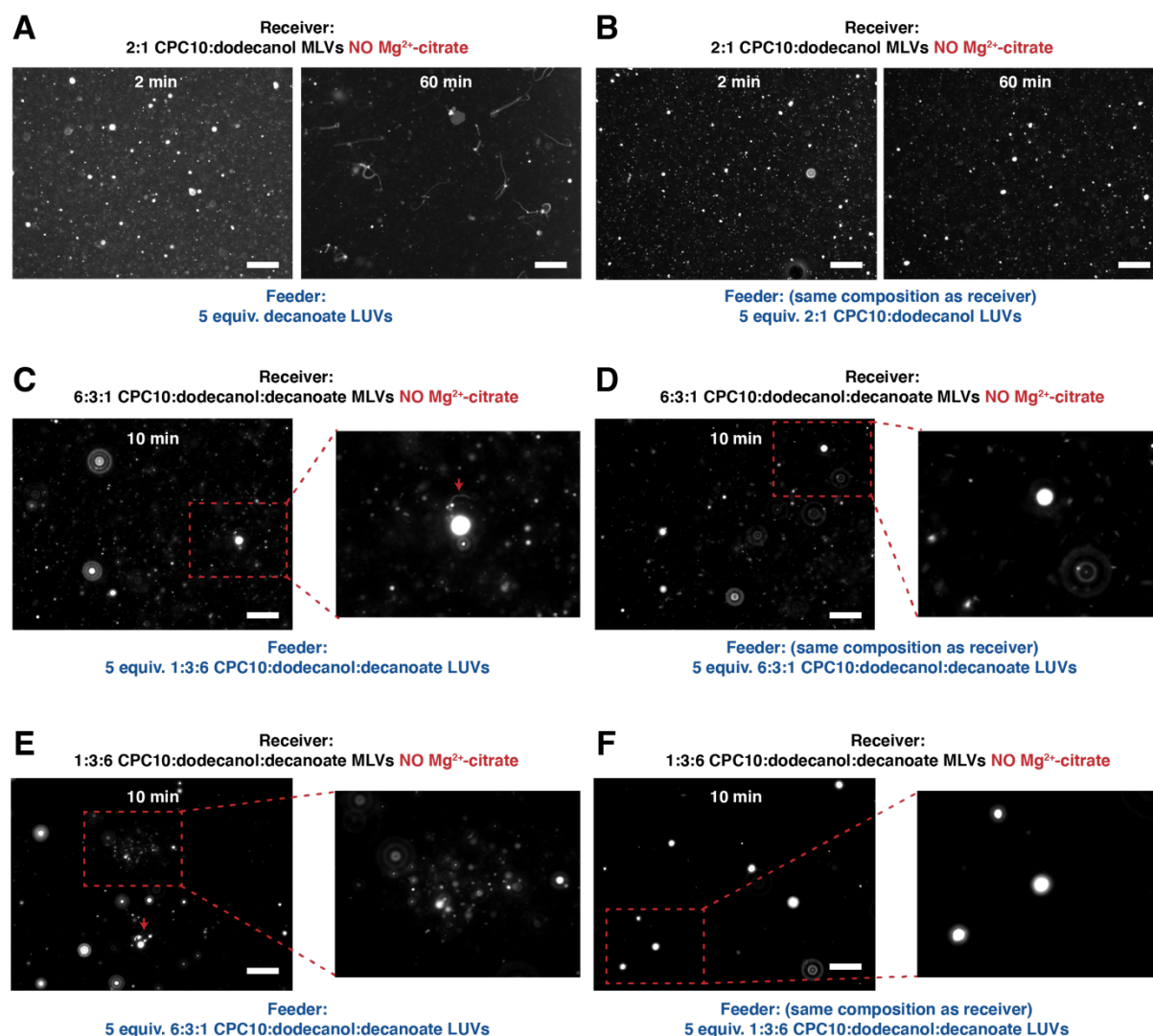


**Figure S18. Growth and division of prebiotically plausible CPC10-based protocells in the absence of Mg<sup>2+</sup>-citrate.**

**(A)** 2:1 CPC10:dodecanol MLVs grew when fed with decanoate LUVs.

**(B)** 2:1 CPC10:dodecanol MLVs did not grow when fed with LUVs of same composition.

**(C)** 6:3:1 CPC10:dodecanol:decanoate (CPC10-rich) MLVs grew when fed with decanoate-rich LUVs.

**(D)** 6:3:1 CPC10:dodecanol:decanoate (CPC10-rich) MLVs did not grow when fed with decanoate-rich LUVs.

**(E)** 1:3:6 CPC10:dodecanol:decanoate MLVs divided when fed with CPC10-rich LUVs.

**(F)** 1:3:6 CPC10:dodecanol:decanoate MLVs did not divide when fed with CPC10-rich LUVs.

All images were taken from different fields and scale bars indicate 20 μm. For fluorescence imaging, the vesicles were labeled with 0.15 mol% LR-DHPE.

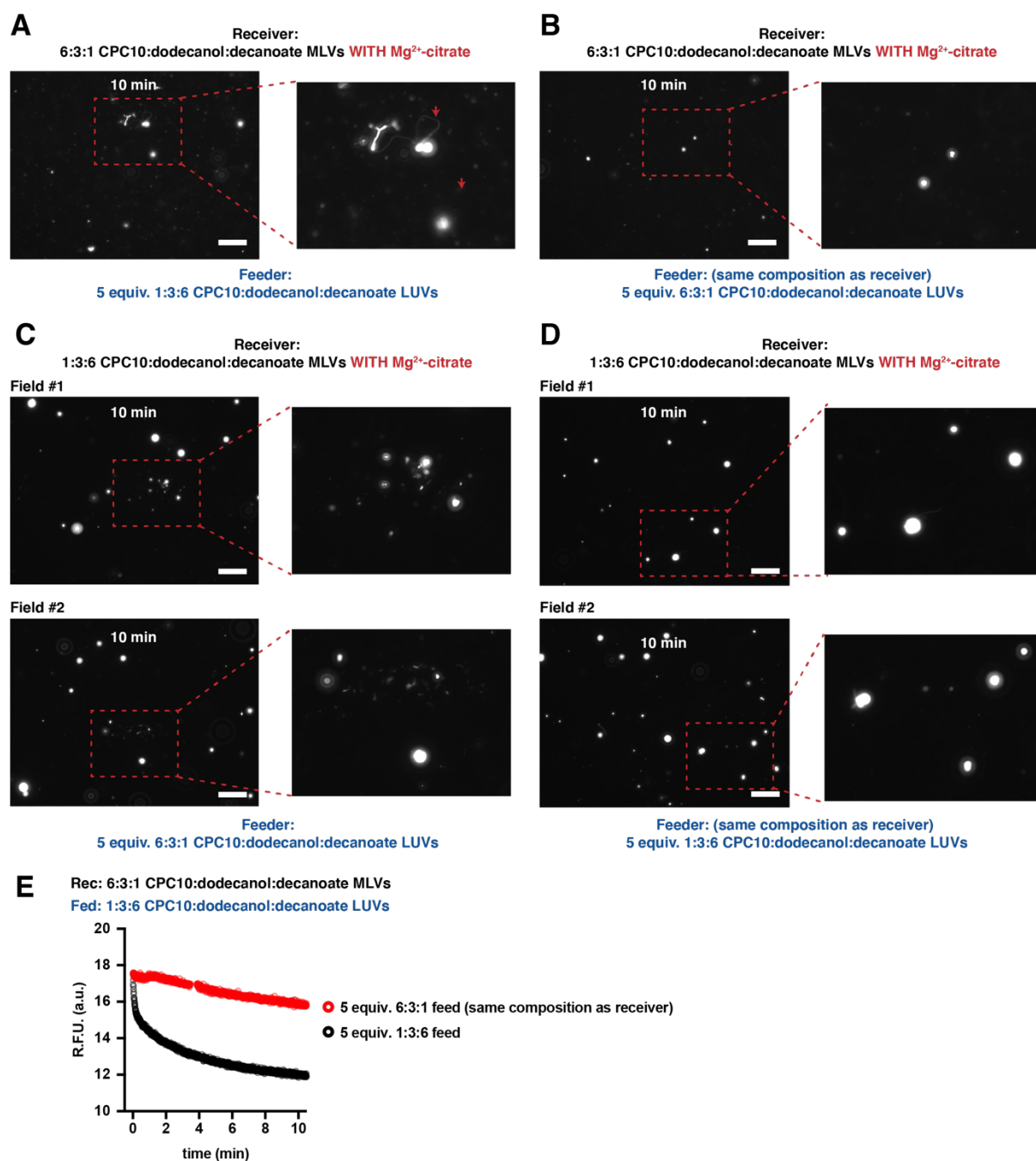


**Figure S19. Growth and division of prebiotically plausible CPC10-based protocells in the presence of Mg<sup>2+</sup>-citrate.**

(A) 6:3:1 CPC10:dodecanol:decanoate (CPC10-rich) MLVs grew when fed with decanoate-rich LUVs.  
(B) 6:3:1 CPC10:dodecanol:decanoate (CPC10-rich) MLVs did not grow when fed with decanoate-rich LUVs.

(C) 1:3:6 CPC10:dodecanol:decanoate MLVs divided when fed with CPC10-rich LUVs.

(D) 1:3:6 CPC10:dodecanol:decanoate MLVs did not divide when fed with CPC10-rich LUVs.

(E) FRET-based vesicle surface area changes of 6:3:1 CPC10:dodecanol:decanoate MLVs.

Mg<sup>2+</sup>-citrate indicates 25 mM Mg<sup>2+</sup>, 100 mM citrate. All images were taken from different fields. Scale bars indicate 20  $\mu$ m. For fluorescence imaging, the vesicles were labeled with 0.15 mol% LR-DHPE.

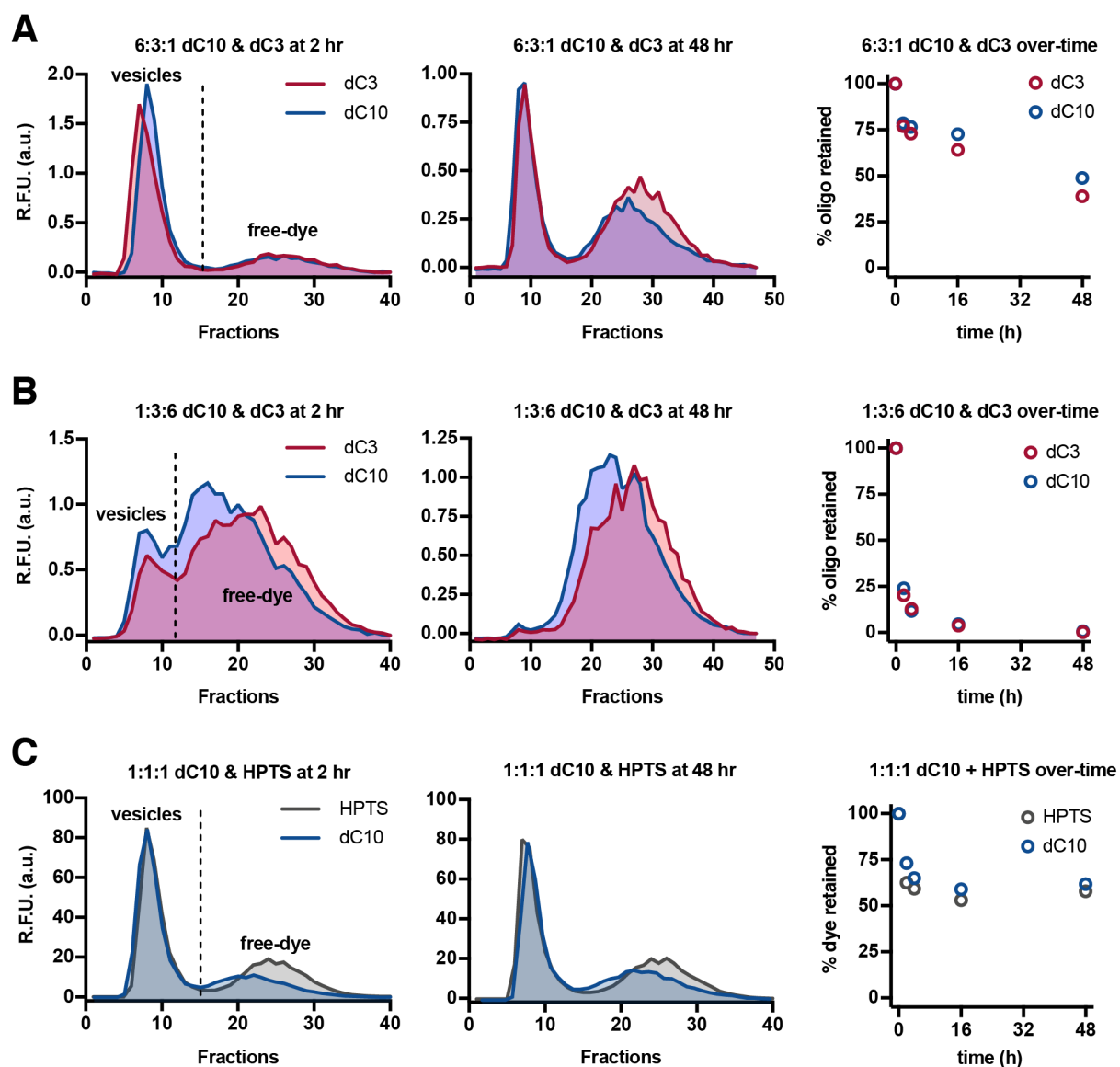


**Figure S20. Release of small molecules and oligonucleotides from protocells.**

**(A)** Stability of 6:3:1 CPC10:dodecanol:decanoate protocells with encapsulated fluorescein-oligo-dC3 and fluorescein-oligo-dC10.

**(B)** Stability of 1:3:6 CPC10:dodecanol:decanoate protocells with encapsulated fluorescein-oligo-dC3 and fluorescein-oligo-dC10.

**(C)** Stability of 1:1:1 CPC10:dodecanol:decanoate protocells with encapsulated HPTS and fluorescein-oligo-dC10.

All experiments were performed in the presence of 25 mM  $Mg^{2+}$ :citrate, pH 8.0.

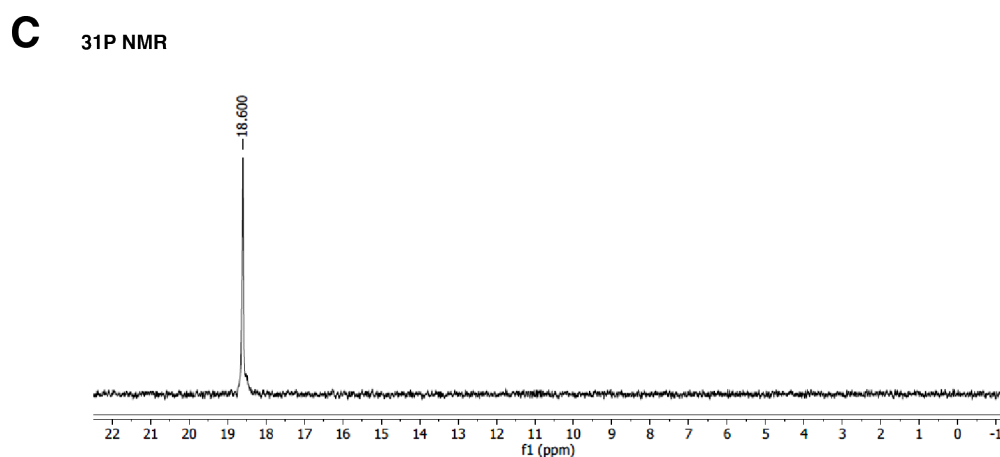
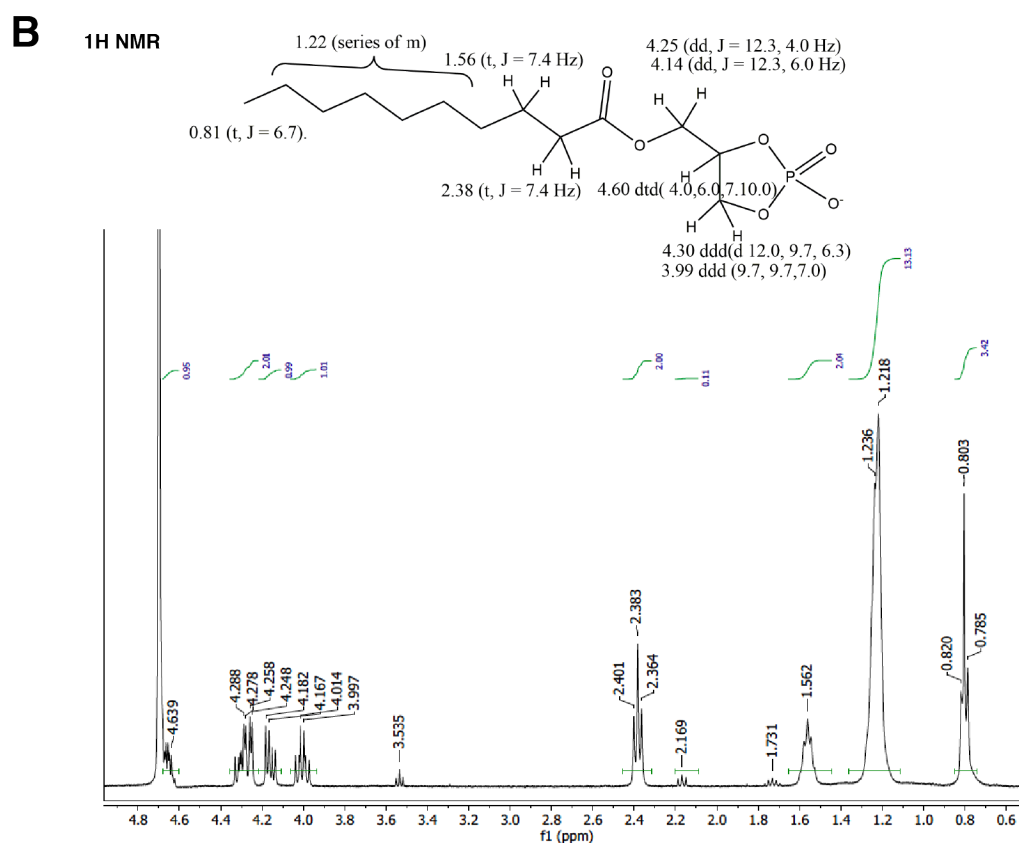
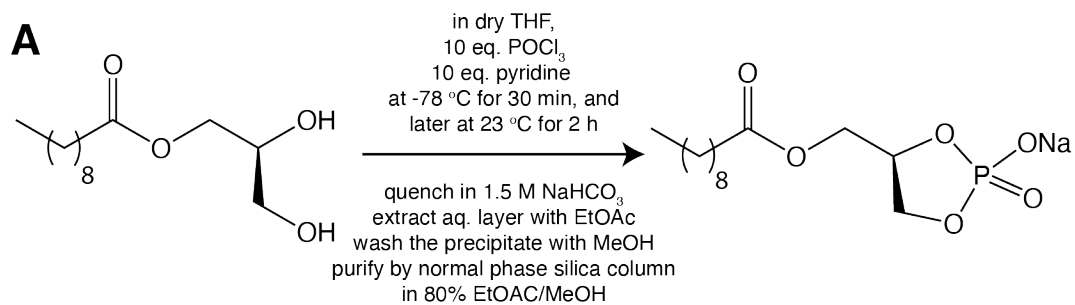


**Figure S21.** NMR analysis of synthesized CPC10.

(A) Overview of synthesis protocol. THF: tetrahydrofuran. EtOAc: ethyl acetate. MeOH: methanol.

(B)  $^1\text{H}$  NMR in  $\text{D}_2\text{O}$ .

(C)  $^{31}\text{P}$  NMR in  $\text{D}_2\text{O}$ , {H-decoupled}.



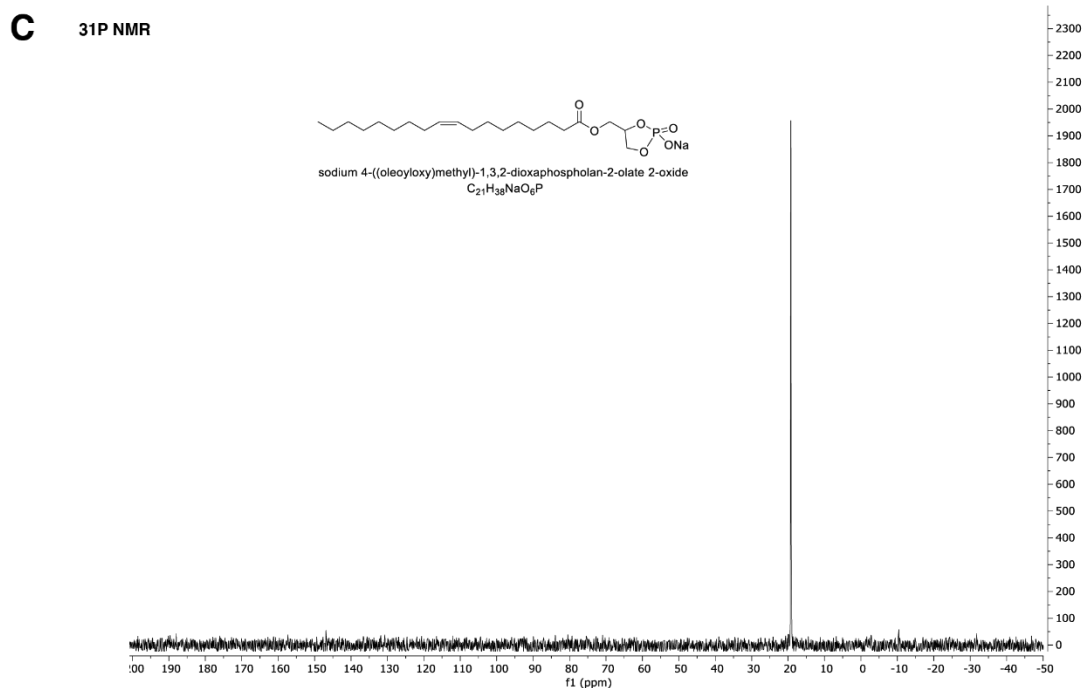
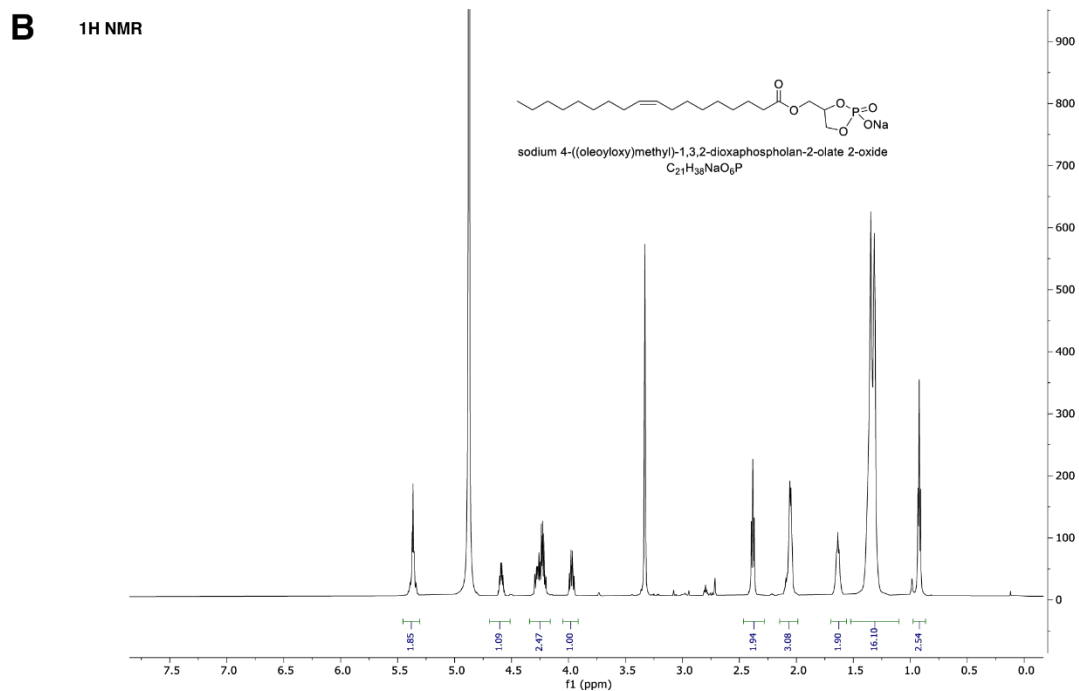
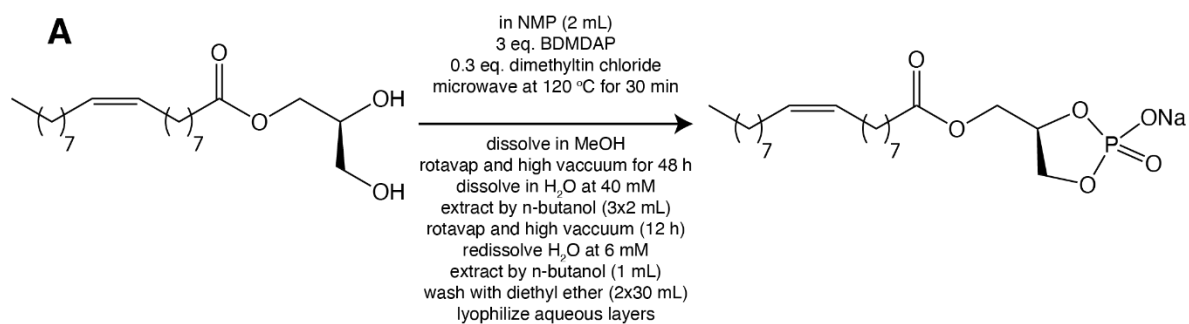


**Figure S22.** NMR analysis of synthesized CPC18.

**(A)** Overview of synthesis protocol. NMP: N-methyl-2-pyrrolidone. BDMDAP: bis(dimethylamino) phosphorodiamidate. MeOH: methanol.

**(B)** <sup>1</sup>H NMR in MeOD. **(C)** <sup>31</sup>P NMR in MeOD, {H-decoupled}.



**Table S1.** List of oligonucleotides and sequences used in this study.

<b>Name</b>	<b>Purpose</b>	<b>Sequence</b>
dC3	Testing vesicle permeability	5'-6-FAM-CCC-3'; where 6-FAM is fluorescein.
dC10	Testing vesicle stability	5'-6-FAM-CCCCCCCCCCC-3'
dA10	Testing vesicle stability	5'-6-FAM-AAAAAAAAAAA-3'
Primer	Nonenzymatic RNA copying	5'-FAM-AGUGAGUACGG-3'
Template	Nonenzymatic RNA copying	3'-UCACUCAUUGCCCCCCTAA-5'